Nanoscale Advances

REVIEW

View Article Online
View Journal | View Issue

Cite this: *Nanoscale Adv.*, 2021, **3**, 1813

The use of amino-based functional molecules for the controllable synthesis of noble-metal nanocrystals: a minireview

Zhijuan Li,† Meng Li,† Xuan Wang, Gengtao Fu * and Yawen Tang *

Controlling the morphologies and structures of noble-metal nanocrystals has always been a frontier field in electrocatalysis. Functional molecules such as capping agents, surfactants and additives are indispensable in shape-control synthesis. Amino-based functional molecules have strong coordination abilities with metal ions, and they are widely used in the morphology control of nanocrystals. In this minireview, we pay close attention to recent advances in the use of amino-based functional molecules for the controllable synthesis of noble-metal nanocrystals. The effects of various amino-based molecules on differently shaped noble-metal nanocrystals, including zero-, one-, two-, and three-dimensional nanocrystals, are reviewed and summarized. The roles and mechanisms of amino-based small molecules and long-chain ammonium salts relating to the morphology-control synthesis of noble-metal nanocrystals are highlighted. Relationships between shape and electrocatalytic properties are also described. Finally, some key prospects and challenges relating to the controllable synthesis of noble-metal nanocrystals and their electrocatalytic applications are proposed.

Received 4th January 2021
Accepted 6th February 2021

DOI: 10.1039/d1na00006c

rsc.li/nanoscale-advances

1. Introduction

Energy crises and environmental pollution brought about by the excessive use of traditional fossil energy sources have urged researchers to explore and utilize new renewable energy sources, such as solar, wind, hydropower, *etc.*[1–4] Thus, establishing effective and sustainable energy conversion and storage systems is extremely important for mankind. Renewable-energy conversion/storage devices, such as fuel cells,[5–10] water electrolysis devices,[11–15] and rechargeable metal-air batteries,[16–20] have attracted widespread attention due to their environmental friendliness, low carbon emissions, and good device safety. Currently, noble-metal-based materials, such as Pt-, Pd-, Ru-, and Ir-based catalysts, are common catalysts for energy-related catalytic reactions,[21–24] including the alcohol oxidation reaction, formic acid oxidation reaction (FAOR), oxygen reduction reaction (ORR), oxygen evolution reaction (OER), hydrogen evolution reaction (HER), and hydrogen oxidation reaction (HOR). However, the scarcities and high prices of noble metals have limited their further commercial application. An attractive

Jiangsu Key Laboratory of New Power Batteries, Jiangsu Collaborative Innovation Center of Biomedical Functional Materials, School of Chemistry and Materials Science, Nanjing Normal University, Nanjing 210023, China. E-mail: gengtaofu@njnu.edu.cn; tangyawen@njnu.edu.cn

† These authors contributed equally to this work.

Zhijuan Li received her B.S. degree from the Department of Chemistry, Bohai University, in 2017. She is currently pursuing her PhD degree at Nanjing Normal University. Her research interests focus on advanced nanomaterials for energy conversion.

Meng Li obtained his B.S. degree from Nanjing Normal University in 2018. Then he joined the School of Chemistry and Materials Science in Nanjing Normal University as a graduate. His current research interests relate to the field of nanostructured materials and their electrocatalytic applications.

strategy to solve this problem is to design catalysts with morphologies, compositions, and surface structures (such as defects and exposed facets) that maximize their mass activities.[25–30]

The mass activity of a noble-metal-based catalyst basically depends on its specific surface area and intrinsic activity.[31–33] A lot of effort has been put into improving the utilization and catalytic activities of noble-metal-based catalysts, such as through reducing particle sizes,[34–36] tuning electronic structures using heteroatoms,[37–40] and selectively exposing highly active facets.[41–47] The shape-controlled synthesis of noble-metal nanocrystals is one of the more significant strategies, considering that the size, morphology, and surface structure are critical for determining the electrocatalytic properties.[22,24,25] Great efforts have been devoted to analyzing the impact of morphology on the electrocatalytic performance of noble metals.[48–50] Noble-metal nanocrystals with specific dimensions (zero-dimensional, one-dimensional, two-dimensional, and three-dimensional)[51,52] and morphologies (ultrafine particles, polyhedra, nanowires, nanosheets, porous structure, *etc.*)[24,41,53,54] show excellent electrocatalytic performance due to their large surface-atom ratios, abundant active sites, and excellent structural stabilities. For example, Xia *et al.*[25] deemed that the construction of special micro-nano-structures, such as nanoframes, nanocages, nanolayers, and core–shell structures, could expose more surface atoms and obtain higher electrochemically active surface areas (ECSAs). Some related research results in recent years also support this viewpoint.[55–60] In addition to structural aspects, the surface state of the catalyst (crystal faces, defects, *etc.*) also has a great impact on the activity of noble-metal nanocrystals.[61–63] Nagahiro Hoshi *et al.*[64] studied the effects of different low-index facets of Pd on catalytic activity during the ORR in an acidic medium. The results showed that the ORR activities of different low-index crystal facets follow the order: Pd(111) < Pd(110) < Pd(100), which is completely opposite to the activity order of different low-index crystal facets of Pt. Wang *et al.*[65] proposed ultra-stable three-dimensional (3D) PtCu nanowires rich in copper vacancy defects that have excellent catalytic performance towards the ORR, and their mass activity is 14.1 times that of a commercial Pt/C catalyst. These theoretical and experimental studies encourage researchers to synthesize catalysts with unique morphologies and surface states, and to study the relationships between their structures and electrocatalytic properties. One of the most critical factors in the synthesis process is the introduction of a morphology-control agent, which can directly affect the structure and surface state of the catalyst.[41]

The use of functional-molecule-mediated complex-reduction methods is an important strategy for the formation of noble-metal nanocrystals with controllable morphologies and surface structures.[66–68] In this method, amino-based functional molecules can be easily used for the controlled synthesis of noble-metal nanocrystals with special structures and morphologies *via* adjusting some factors. In addition, amino-based functional molecules may affect the electronic state of noble-metal nanocrystals and may possess unique steric-hindrance effects, thereby affecting the electrocatalytic activity, stability,

Xuan Wang achieved his B.S. degree at Xuzhou University of Technology in 2016. Then he joined the School of Chemistry and Materials Science in Nanjing Normal University as a graduate. His research interests relate to the design of nanostructured materials with electrocatalytic applications and theoretical simulations.

Gengtao Fu received his PhD from the School of Chemistry and Materials Science at Nanjing Normal University in 2017. He spent one year (2015–2016) as a visiting scholar at the University of Texas at Austin. He was a research fellow at Nanyang Technological University working with Prof. Jong-min Lee (2017–2019). Then he worked at the University of Texas at Austin with Prof. John B. Goodenough (2019–2020). He currently works at the College of Chemistry and Materials Science at Nanjing Normal University. His current research interests relate to the area of nanostructured electrocatalysts and their applications in energy storage and conversion.

Yawen Tang received his BS degree and MS degree from Nanjing Normal University in 1992 and 2002, respectively, and his PhD from Nanjing University of Science & Technology in 2011. He is currently a professor at the College of Chemistry and Materials Science at Nanjing Normal University. His main research interests relate to the synthesis and assembly of nanomaterials and their applications in batteries, fuel cells, and photocatalysis.

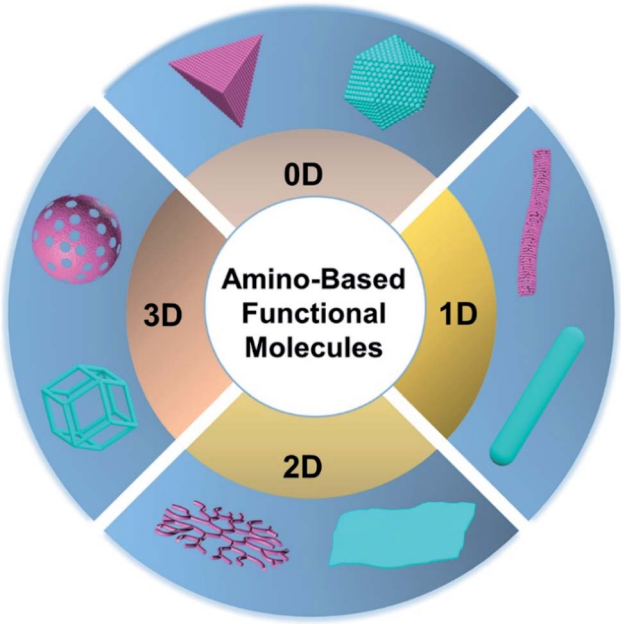

Scheme 1 A schematic illustration of the role of amino-based functional molecules during morphology formation.

and selectivity of catalysts.[69,70] In this minireview, we aim to offer an update on emerging recent research progress relating to the use of amino-based functional molecules in the controllable synthesis of noble-metal nanocrystals in the field of electrocatalysis. The noble-metal nanocrystals are divided into zero-dimensional, one-dimensional, two-dimensional, and three-dimensional structures. The roles and effects of amino-based functional molecules on the morphology formation of noble-metal nanocrystals are emphasized (Scheme 1). The relationships between morphologies and electrochemical properties are described, and the corresponding mechanisms are explained. An in-depth understanding of the mechanism of preferential adsorption of amino-based functional molecules is significantly important for designing noble-metal nanocrystals with desired electrocatalytic performances in the future.

2. Amino-based functional molecules

The amino group is one of the basic base groups in organic chemistry. Depending on the group (R-) to which the amino group is connected, amino-based functional molecules can be classified into different types. If R- is a long-chain organic group, it is called a polymeric amine (such as polyacrylonitrile and poly(allylamine hydrochloride)), and when R- is a small molecule, it is called a small molecular amine (ethylenediamine, triethanolamine, urea, *etc.*). Depending on the number of amino groups, they can be classified as amines, diamines, triamines, *etc.* Amino-based functional molecules are widely used to synthesize various morphologies because of their unique advantages, as follows: (i) nitrogen in an amino-based molecule has strong abilities to coordinate with metal cations, which can affect the reduction sequence of metal precursors; (ii) amino-based molecules can be used to assist the nucleation and growth rates of high-exponent nanocrystals through kinetic control; (iii) under thermodynamic control, amino-based molecules with different aliphatic chains can be adsorbed on specific crystal surfaces to synthesize variously shaped noble-metal nanocrystals; and (iv) amino-based molecules are susceptible to pH and can be used as bubble templates to construct hollow or porous structures.[71,72] For example, urea is a temperature-sensitive amino-based molecule that can be

Table 1 Recent 0D, 1D, 2D, and 3D nanostructures synthesized with amino-based molecules

Dimension	Amino-based molecule	Nanostructure	Ref.
0D	NH_3	Pd tetrahedra	80
	Glycine	Pt–Ni–Cu nanocrystals	81
	Glycine	Pt-based tetrahexahedra	82
	Octadearyl dimethyl ammonium chloride	Au–Pd hexoctahedra	83
	L-Proline	PtCo nanoassemblies	84
	L-Glutamic acid	PtPd@Pt core/satellites	85
	Arginine	PtCu nanoassemblies	86
	Glycine	PtCoRh nanoassemblies	76
1D	Poly-L-lysine	Pd networks	87
	3-Amino-propyltriethoxysilane	Pt nanoarrays	88
	N,*N*-Dimethylformamide	Pt_3Ni nanowires	89
	Hexadecyl trimethyl ammonium chloride	$PtNi_{1.21}Pd_{1.36}$ nanowires	90
	Hexadecyl trimethyl ammonium chloride	Pt–Ni nanowires	91
	Hexadecyl trimethyl ammonium chloride	Pt-based nanowires	92
2D	Oleylamine	PdMo bimetallene	38
	$C_{22}N$–COOH	Pt–Ru nanodendrites	93
	Tris(hydroxymethyl) aminomethane	PtCu@Pd nanoplates	94
	Oleylamine	Pd nanosheets	95
3D	Dioctadecyldimethylammonium chloride	Porous PdAgCu	96
	Dioctadecyldimethylammonium chloride	Porous PdAgCu	97
	Glycine	PtCu nanoframes	79
	Oleylamine	Pt_3Ni nanoframes	98

decomposed to produce a large amount of CO_2 and NH_3 bubbles ($CO(NH_2)_2 + H_2O \rightarrow 2NH_3 + CO_2$) at a certain temperature, and it can serve as an original soft template to induce the formation of hollow- or bowl-shaped noble-metal nanocrystals.[48,73,74] In addition, the usage of different functional groups to modify the R-group can be used to adjust and optimize the reduction order of metal ions and regulate the rates of reduction reactions. A good example of this is amino-acid molecules, which have various kinds of functional groups and have adjustable coordination abilities with metal ions. Thus, the targeted synthesis of nanocrystals with special morphologies and compositions is possible through the appropriate selection of and modulation with amino-acid molecules (Table 1).[75–79]

3. Differently shaped noble-metal nanocrystals

3.1 Zero-dimensional (0D) structures

Zero-dimensional (0D) materials with small particle-sizes and different shapes can function as effective electrocatalysts due to the size effect and surface effect. The atomic utilization efficiency of noble-metal nanocrystals will increase as the size of

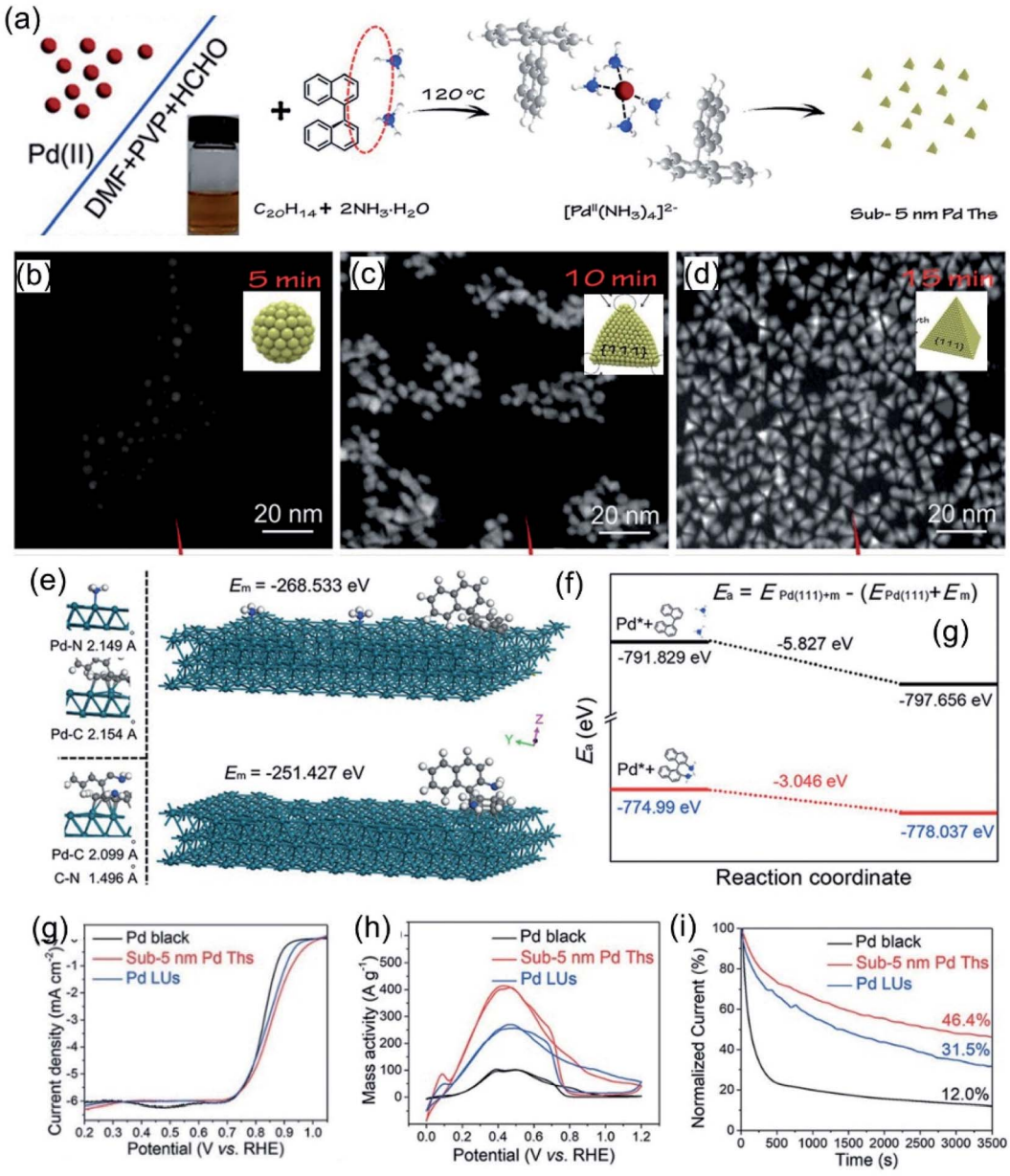

Fig. 1 (a) A schematic illustration of the formation of sub-5-nm Pd tetrahedrons. (b–d) HAADF-STEM images of sub-5-nm Pd tetrahedrons recorded at different synthesis stages. Schematic illustrations of typical adsorption processes (e) and diffusion paths (f) involving $C_{20}H_{14}$ + $2NH_3$ and $C_{20}H_{16}N_2$ on Pd(111). (g) ORR polarization curves recorded in an O_2-saturated 0.1 M KOH solution. (h) CV curves in 0.5 M H_2SO_4 + 0.5 M HCOOH solution. (i) Chronoamperometric curves at 0.4 V. Copyright: 2020, Wiley.[80]

the nanocrystals shrinks.[99] For example, the atomic utilization efficiency of Pt nanoparticles increases from 9.5% to 26% when the side length of cubic Pt nanoparticles is reduced from 11.7 to 3.9 nm.[25] As discussed by Nesselberger[100] and Yuan *et al.*,[101] nanoparticles with ultra-small size are rich in surface atoms, showing strong electronic effects and a high surface bond density in suspensions, endowing them with high electrocatalytic activity. However, it is still a huge challenge to directly synthesize ultra-small nanocrystals with specific shapes and crystal facets.[102] Precise control of the reaction kinetics may be a possible means to synthesize ultra-small nanocrystals.[103,104] Adjustments to the dispersion state between amino groups and other additive molecules (whether they form bonds) can be used to directly adjust the thermodynamics and kinetics of the reaction system, thereby inducing the formation of noble-metal nanocrystals with distinctive morphologies.

Ammonia is the simplest amino molecule, and it can coordinate with metal ions to form complexes, thus reducing the initial reduction potential. Zhang *et al.*[80] reported sub-5-nm Pd nanocrystals *via* an effective NH_3-mediated process. As shown in Fig. 1a, negatively charged $PdCl_4^{2-}$ ions were bound by $C_{20}H_{14}$ (1,1′-binaphthalene) + $2NH_3$ to produce a $[Pd^{II}(NH_3)_4]^{2-}$ complex. The final product was obtained upon further heating. Time-dependent evolution experiments were used to investigate the structural evolution process of the sub-5-nm Pd nanocrystals (Fig. 1b–d). With the extension of time, the sample gradually changed from irregular small particles with a size of 2 nm to a quasi-spherical structure with micro-rounded corners; then, the rounded corners began to sharpen and finally a complete tetrahedron shape with a size of 5 nm was formed. The growth mechanism of the tiny particles can be attributed to strong adsorption and a relatively fast reduction rate, which can force Pd to grow into thermodynamically controlled products

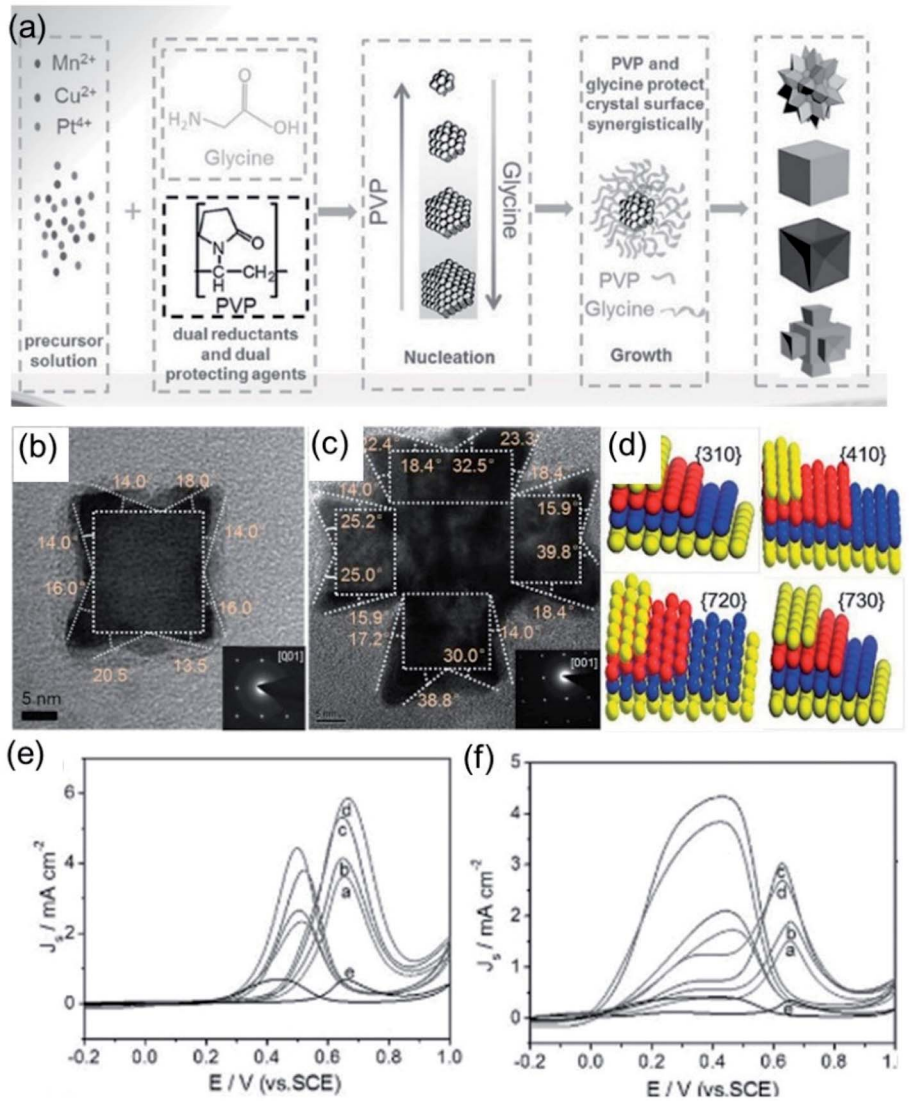

Fig. 2 (a) Schematic illustrations of Pt-based alloy NPs. (b) TEM and SAED (inset) images of a single PtMnCu CNC. (c) TEM and SAED (inset) images of a single PtMnCu RP. (d) Models of the {310}, {410}, {720}, and {730} facets of *fcc* Pt. (e) CV curves in 0.5 M H_2SO_4 + 2 M CH_3OH. (f) CV curves in 0.5 M H_2SO_4 + 0.25 M HCOOH. Copyright: 2017, Wiley.[47]

with a low surface energy. Density functional theory (DFT) calculations (Fig. 1e and f) indicate the adsorption energy difference between two kinds of additives with different bonding states on the Pd(111) surface, resulting in two distinct product morphologies. The results show that the adsorption of $C_{20}H_{14} + 2NH_3$ molecules on Pd(111) is relatively strong, with an adsorption energy of −5.827 eV, while the adsorption of $C_{20}H_{16}N_2$ molecules on Pd(111) is weak, with an energy of only −3.046 eV. The strong adsorption between $C_{20}H_{14} + 2NH_3$ and Pd(111) could weaken the chemical bonding inside Pd(111), leading to a decrease in the activation energy and speeding up the reduction rate of Pd, which facilitates the formation of sub-5-nm Pd tetrahedrons. Obviously, the reaction system involving $C_{20}H_{14} + 2NH_3$ exhibits faster reduction kinetics, which is consistent with the DFT calculation results. Compared with laciniate Pd nanourchins (Pd LUs) and commercial Pd black, sub-5-nm Pd tetrahedrons (Ths) showed the best activity and stability in both basic ORR tests and FAOR tests, which could be attributed to the ultrasmall size with a larger specific surface area (Fig. 1g–i).

The surface state of a catalyst depends on the atomic arrangement and coordination number of the exposed surface.[105,106] The intrinsic activity of the active sites is related to the coordination number of the exposed facet.[107] Taking the face-centered cubic (*fcc*) crystal structure as an example, the surface facets can be divided into low-refractive-index facets, including the (100), (110) and (111) facets, and high-index facets.[51,93] The design of noble-metal nanocrystals with exposed high-index facets is an effective strategy to improve electrocatalytic performance. Amino acids with both amino and carboxyl groups are widely used in the synthesis of noble-metal nanocrystals due to their selective coordination abilities with metal ions. Strong interactions between amino and carboxyl groups through hydrogen bonding and electrostatic interactions can effectively drive the self-assembly of noble-metal nanocrystals.[60,86] Glycine is one of the most commonly used amino acids, containing a carboxyl group and amino group that can interact with metal ions to generate complexes, followed by the synthesis of electrocatalysts with various morphologies. For instance, Zhang *et al.*[47] developed a general approach for preparing Pt-based alloys with high-index facets using glycine and poly(vinylpyrrolidone) (PVP) as dual capping and reducing agents (Fig. 2a). The effect of glycine was comprehensively studied *via* changing the content levels in the standard synthetic process. Owing to close coordination between the metal precursor and glycine, the reduction rate of the metal precursor becomes slower with an increase in the glycine content. In this instance, the nucleation rate slows down and, thus, the number of crystal seeds obtained decreases. Since a smaller amount of metal precursor is consumed in the nucleation stage, the growth rate of seeds is accelerated after the formation of crystal nuclei. Therefore, the size of the

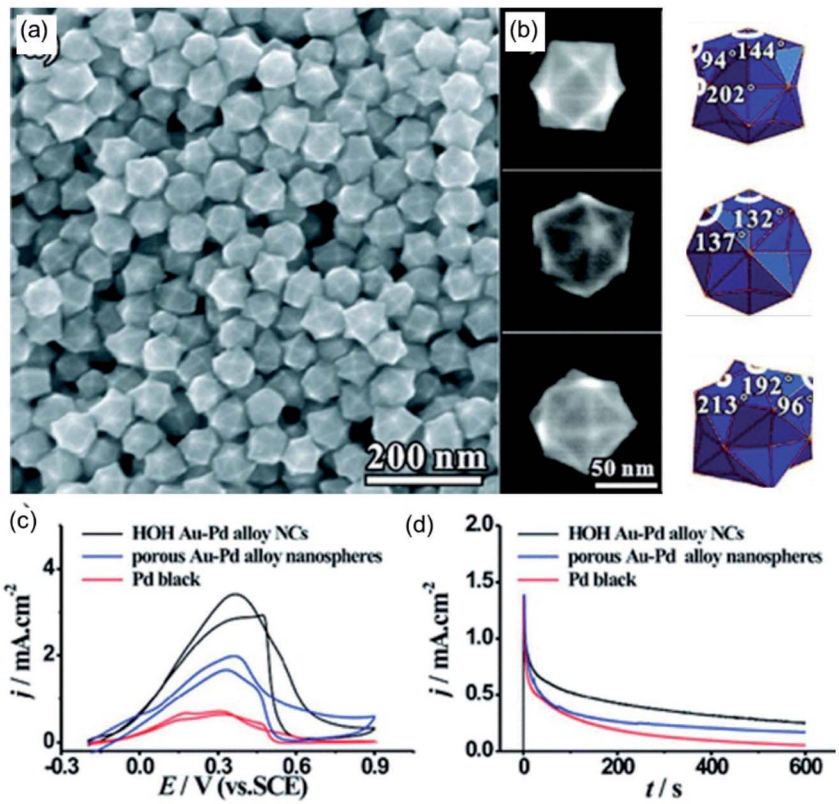

Fig. 3 (a) An SEM image of HOH AuPd alloy NCs. (b) High-magnification SEM images and corresponding models of the HOH NCs. (c) CV curves in 0.50 M H_2SO_4 + 0.25 M HCOOH. (d) Chronoamperometric curves at 0.4 V. Copyright: 2011, ACS.[83]

synthesized particles increases with an increase in the amount of glycine after the same reaction time. Moreover, under the same reaction conditions, the morphology of the Pt-based alloy particles changed significantly in the presence of different amounts of glycine. *Via* suitably optimizing the amounts of glycine and PVP, four kinds of catalysts, PtMnCu nanocubes (NCs), PtMnCu concave nanocubes (CNCs), PtMnCu nanoflowers (NFs) and PtMnCu ramiform polyhedrons (RPs), with uniform size were synthesized effectively. The PtMnCu RPs and CNCs were bound by high-index facets (Fig. 2b and c). The crystal index of the high-index facets was determined *via* selective-area electron diffraction (SAED). The results show that the PtMnCu RP catalyst was enclosed by HIFs, such as {410}, {720}, {310}, and {730} (Fig. 2d). These four catalysts were applied to the methanol oxidation reaction (MOR) (Fig. 2e) and formic acid oxidation reaction (FAOR) (Fig. 2f). Compared with commercial Pt black, these four catalysts all showed excellent catalytic activity, among which the PtMnCu RP catalyst showed the best specific activity due to its high-index facets.

In addition to amino-based functional small molecules, long-chain macromolecular ammonium salts can also assist in the synthesis of polyhedrons with high-index facets. Xie *et al.*[83] synthesized hexoctahedral (HOH) Au–Pd alloy nanocrystals with {*hkl*} high-index facets with the assistance of octadecyl trimethyl ammonium chloride (OTAC). As shown in Fig. 3a, the as-prepared catalyst was composed of a well-defined structure with high purity. The hexoctahedral (HOH) shape was observed from different orientations in SEM images, agreeing with schematic models (Fig. 3b). The {431} high-index facets of the HOH shape are also deduced based on outlines, angles, and corresponding SAED analysis. To investigate the effects of OTAC on the morphology of the hexoctahedral (HOH) Au–Pd alloy nanocrystals, controlled experiments were performed without OTAC, where the HOH shape could not be formed. This result further indicates that OTAC acts as a morphology regulator in the synthesis reaction. The FAOR was used to prove the electrocatalytic activity and stability of the as-prepared HOH Au–Pd alloy nanocrystals. Compared with control samples, the HOH Au–Pd alloy nanocrystals showed the best electrocatalytic activity and stability towards the FAOR owing to the high-index facets and a synergistic effect between Au and Pd (Fig. 3c and d).

3.2 One-dimensional (1D) structures

Compared with 0D nanoparticles, 1D nanostructures, especially ultrafine nanowires with highly anisotropic structures, possess unique structural advantages, including plentiful active sites and boosted electron and mass transport.[108–110] Some studies have signified that 1D nanowires of Pt, Au, Ru, Ir, Rh, and Pd catalyst have better electrocatalytic activity and durability properties than 0D nanoparticles.[92,108,109] Although 1D nanowires have these advantages, their extensive practical application is restricted by issues relating to synthetic methods. Among

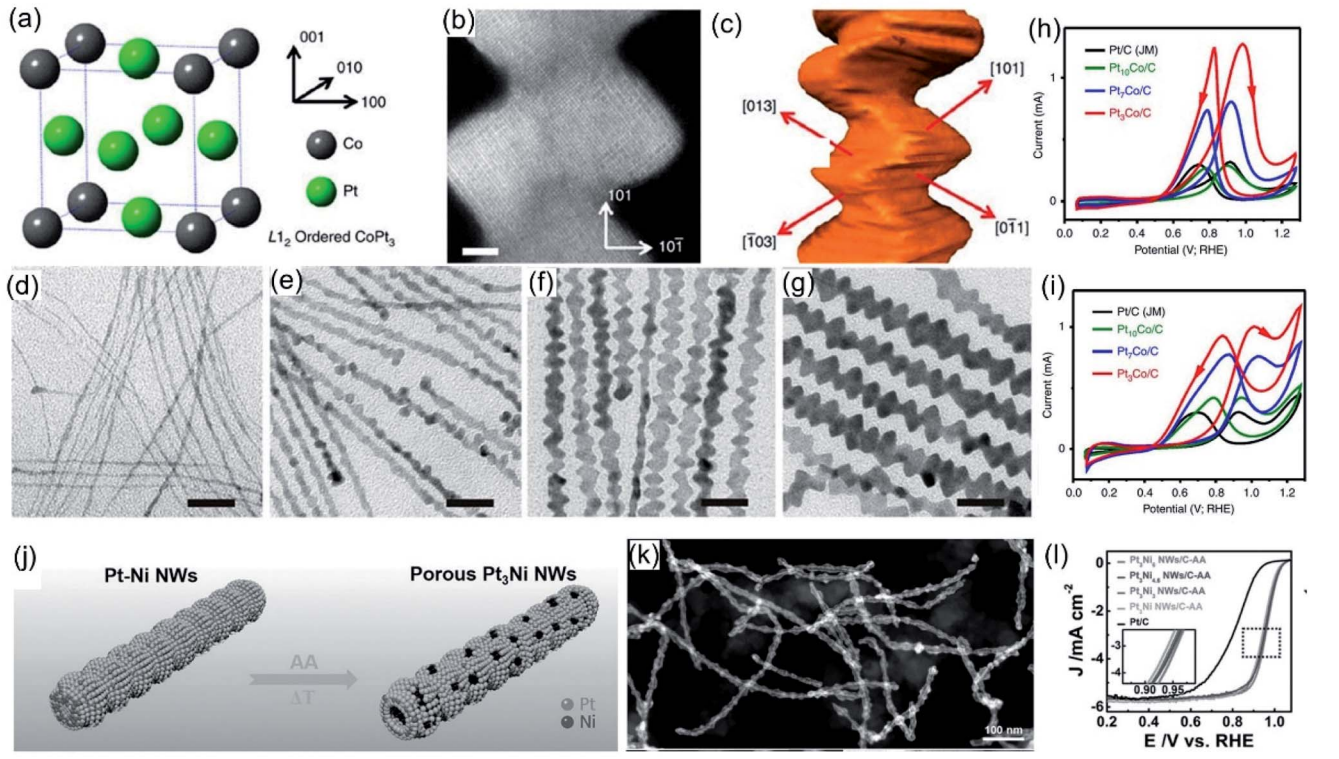

Fig. 4 (a) A schematic diagram of the L1$_2$-ordered intermetallic structure of Pt_3Co. (b) An atomic resolution HAADF-STEM image and (c) indices of the flat planes of Pt_3Co NWs. (d–g) TEM images of hierarchical Pt_3Co NW intermediates. (h) CV scans in 0.1 M $HClO_4$ + 0.2 M methanol. (i) CV scans in 0.1 M $HClO_4$ + 0.2 M ethanol. Copyright: 2016, Nature.[126] (j) A schematic presentation of porous Pt_3Ni NWs. (k) A HAADF-STEM image of porous Pt_3Ni NWs. (l) ORR polarization curves in 0.1 M $HClO_4$. Copyright: 2017, Wiley.[91]

the various synthetic methods, ligand-assisted methods, especially those involving amino-based ligands, are widely used and play a central role in the synthesis of 1D nanowire structures because their unique functional groups can show different combination strengths with metal atoms/ions and different surface preferences. Commonly used ionic amino-based ligands, including cetyltrimethylammonium chloride (CTAC),[111–115] cetyltrimethylammonium bromide (CTAB),[116–120] octadecyltrimethylammonium chloride (OTAC),[112,121] and dioctadecyldimethylammonium chloride (DODAC),[122–125] are usually composed of a hydrophilic group and a hydrophobic long carbon chain, which can effectively coordinate with metal ions/atoms, thus adjusting crystal growth during the growth process. Compared with ionic amino-based ligands, organic amino-based ligands, such as oleylamine (OAm), dimethylformamide (DMF), and dimethylacetamide (DMA), have weaker attachment strengths with metal ions/atoms, which can limit the evolution of metal nanocrystals and lead to the formation of well-defined nanowires. Huang *et al.*[126] used CTAC and OAm to successfully synthesize hierarchical PtCo nanowires. Because the local order corresponds to the $L1_2$-ordered intermetallic structure, the projected $L1_2$ unit of Pt_3Co is a face-centered cubic structure consisting of ordered Pt and Co (Fig. 4a). Comprehensive results based on HAADF-STEM images (Fig. 4b) and electronic tomography (Fig. 4c) show that hierarchical Pt_3Co nanowires contain many rough and high-energy active surfaces, such as [310]. To explore the growth mechanism of layered nanowires, intermediates obtained after different reaction times were monitored (Fig. 4d–g). Combining TEM images and XRD results, ultrathin Pt nanobelts were seen to form in the initial stage. With the extension of time, the surface of the nanobelts gradually becomes rough and then a layered structure appears, thus obtaining typical hierarchical nanowires. Based on the exploration of the formation mechanism, it can be inferred that Pt and Co have different reduction potentials and diffusion rates as a result of help from CTAC and OAm, which leads to the synthesis of hierarchical nanowires. As an electrocatalyst for both the MOR and EOR, the obtained

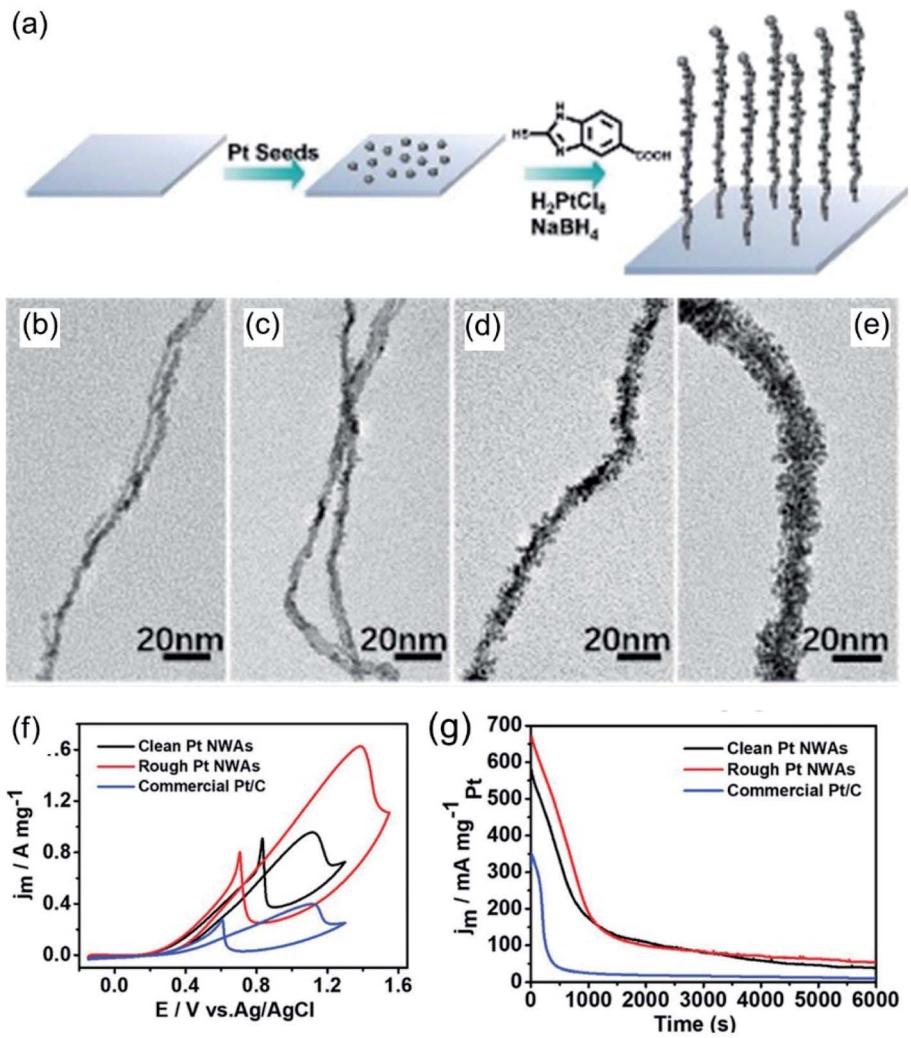

Fig. 5 (a) A schematic illustration of a Pt NWA. (b–e) Typical TEM images of hierarchical platinum nanowire intermediates. (f) CV curves in 0.1 M $HClO_4$ + 0.5 M CH_3OH. (g) CA curves at 0.80 V *versus* Ag/AgCl. Copyright: 2020, Wiley.[88]

Pt_3Co nanowires showed outstanding electrochemical activity (Fig. 4h and i). Huang *et al.*[91] also effectively synthesized porous PtNi nanowires (Fig. 4j). SEM imaging exhibited the well-defined nanowires with a hollow and porous structure (Fig. 4k). The as-prepared porous Pt_3Ni NWs exhibited remarkable ORR activity due to their hollow porous structure and high-index facets (Fig. 4l).

Apart from the above-mentioned amino-based molecules, there are many other kinds of amino-based molecules that can be used to regulate nanowires. Wang *et al.*[88] used 3-aminepropyltriethoxysilane (APTES) and 2-mercapto-5-benzimidazolecarboxylic acid (MBIA) to assist in the synthesis of Pt nanowire arrays and explored the effects of MBIA on rough Pt nanowires through time-based control experiments (Fig. 5a–e). Compared with smooth Pt nanowires and commercial Pt/C, the rough Pt nanowires showed the best electrochemical activity and stability for the MOR in an acid medium (Fig. 5f and g). Huang *et al.*[127] prepared an ultrathin Pt multiple-twinned nanowire network (MTNN) with the assistance of the amino-acid sequence Ac-TLHVSSY-$CONH_2$ (BP7A). An investigation of the reaction kinetics showed that the nanowire network gradually evolved from nanoparticles. Experimental results examining controlling variables showed that the concentration of BP7A peptide plays a key role in the formation of nanowires. Nanowires were obtained at a relatively high peptide concentration, while only nanoparticles were observed at a low peptide concentration. This may be due to stronger constraints on the initial particles and stronger molecular interactions between peptides driving the assembly process at higher peptide concentrations. A large number of double defects was observed in the final product, indicating that the existence of peptide molecules enhances and retains lattice mismatches; this may be due to the stable specificity of BP7A peptide toward double-site binding. Owing to the unique structural features, the Pt MTNN was evaluated as an ORR and MOR electrocatalyst in acidic media. Compared with commercial catalysts, the Pt MTNN showed improved activities toward both the ORR and MOR.

3.3 Two-dimensional (2D) structures

Another way to increase the utilization efficiency of noble-metal nanocrystals is to assemble them into two-dimensional (2D) nanostructures.[52,128,129] 2D materials have attracted widespread attention for electrocatalytic applications because of their high specific areas, high surface-to-volume ratios, and fast electron-transfer rates.[61,130,131] The atomic utilization efficiency of nanosheets will increase as the thickness decreases. Theoretically, when the thickness of a nanosheet reaches only two atomic layers, the atom utilization efficiency can reach 100%.[25]

One of the most efficient methods for the controllable synthesis of nanosheets is restricting the growth of nanocrystals through the selective adsorption of surfactants.[25] Owing to the good coordination abilities of N atoms, amino-based molecules can easily coordinate with metal ions and act as good coordination ligands. In addition, amino-based surfactants with long hydrophobic chains can be assembled into lamellar structures, acting as soft-templates for the synthesis of 2D nanosheets. For example, Xu *et al.*[93] demonstrated that the long-chain amphiphilic surfactant $C_{22}H_{45}$–$N^+(CH_3)_2CH_2COOH(Br^-)$ (denoted as C_{22}N–COOH) has both a hydrophobic chain and a functionalized hydrophilic group, and it could easily assemble into lamellar micelles (Fig. 6a). In addition, the coordination of positively charged ammonium and negatively charged noble-metal-based precursors could lead to the formation of lamellar organic–inorganic hybrids, which is helpful for the growth of PtRu nanocrystals along the plane direction. PtRu NDs exhibited a highly branched planar structure with an average size of about 150 nm (Fig. 6b–d). Time-dependent evolution experiments (Fig. 6e–h) indicate that the nanodendrite formation process follows an epitaxial growth mechanism. Owing to the 2D branched morphology and controlled bimetallic composition, the as-prepared PtRu NDs exhibit 1.3-fold and 3.2-fold increases in ECSA and mass activity compared to commercial Pt/C for the MOR reaction in 1.0 M KOH + 1.0 M methanol (Fig. 6i–l).

Recently, 1-oleylamine has been widely employed as a solvent or dispersant for the synthesis of 2D noble-metal-based nanomaterials. Wang *et al.*[95] reported ultra-thin Pd nanosheets *via* an ionic layer epitaxy (ILE) method with the assistance of 1-oleylamine. As shown in Fig. 7a, ionized 1-oleylamine molecules self-assemble into a positively charged monolayer at the water–air interface, acting as a soft-template, while negatively charged anionic groups (such as $PdCl_4^{2-}$) could adsorb on the interface forming an ultrathin pre-polymerization zone below the monolayer. Therefore, the as-prepared Pd nanosheets exhibit ultrathin characteristics, being only 2.3 nm thick (Fig. 7b). Due to their extremely thin thickness, high crystallinity, and exposed active crystal facets, the Pd nanosheets exhibited extremely high catalytic activity for the FAOR in 0.5 M H_2SO_4 + 0.25 M HCOOH, 30 times higher than that of commercial Pd black. Guo *et al.*[38] reported ultrathin PdMo nanosheets *via* a one-pot wet chemical method using 1-oleylamine as a solvent and dispersant. The as-synthesized PdMo bimetallene nanosheets consist of 2D ultrathin flexible nanosheets with a size of about 100 nm and a thickness of about only 0.88 nm (Fig. 7c and d), which is about the thickness of 4 atomic layers. Electrochemical tests show that PdMo bimetallene is an efficient and stable catalyst for both the ORR and OER. Benefiting from its ultrathin structure, as-synthesized PdMo bimetallene exhibited a high electrochemically active area, high atom utilization, and large mass specific activity in alkaline electrolyte at 0.9 V (16.37 A mg^{-1}_{Pd}), 78 and 327 times higher than those of Pt/C and Pd/C catalysts, respectively (Fig. 7e and f). Apart from the intact ultrathin nanosheets, 2D ultrathin nanodendrites with rich channels could expose abundant active sites, providing efficient mass transfer paths during the electrocatalytic process.

3.4 Three-dimensional (3D) structures

Noble-metal nanocrystals with typical 3D nanostructures, like porous structures, frame structures, and dendrite structures, have motivated widespread research interest over the past few

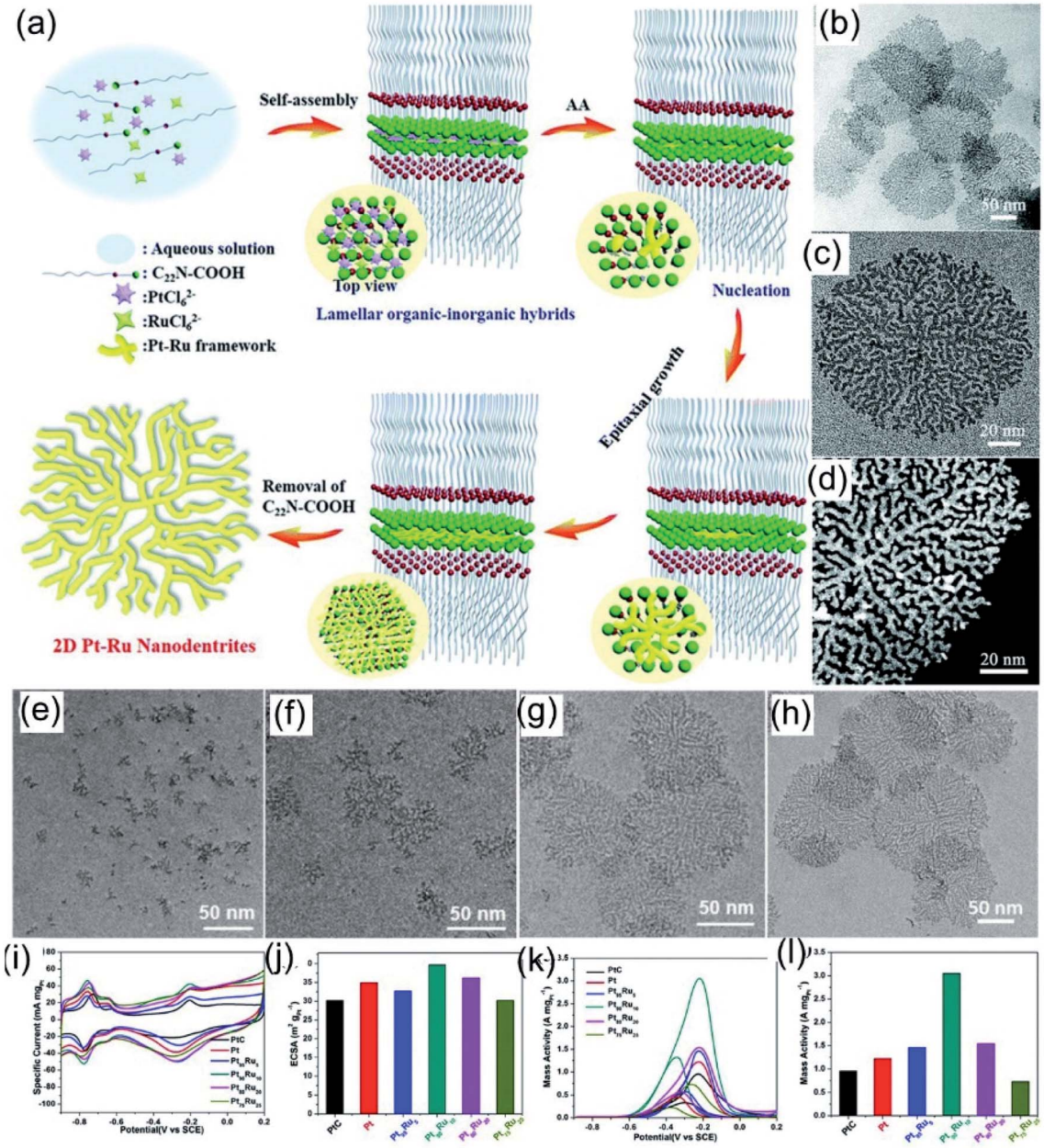

Fig. 6 (a) A schematic illustration of ultrathin Pt–Ru NDs. (b) Low- and (c) high-magnification TEM images of ultrathin Pt–Ru NDs. (d) A low-magnification high-resolution HAADF-STEM image of ultrathin Pt–Ru NDs. (e–h) Typical TEM images of Pt–Ru nanostructures at different crystalline stages. (i) CV curves in 1.0 M KOH and (j) calculated ECSAs. (k) CV curves and (l) calculated mass activities in 1.0 M KOH + 1.0 M CH_3OH. Copyright: 2019, RSC.[93]

decades.[129,132,133] Compared with other methods, the template-assisted method has unique advantages for the synthesis of 3D noble-metal nanocrystals.[134–137] The construction of 3D nanostructures, such as porous and hollow nanostructures, could be carried out with the assistance of molecular templates, such as amphiphilic surfactants.[138,139] Amino-based groups are typical hydrophilic groups that could act well as amphiphilic surfactants for the synthesis of hollow and porous structures. As a typical example, Liu *et al.*[97] reported the synthesis of hollow mesoporous PdAgCu nanospheres with dioctadecyldimethylammonium chloride (DODAC) as the "dual"-templating/structure-directing agent. The amphiphilic surfactant DODAC has a hydrophilic head and two hydrophobic tails, and it could self-assemble into rod and vesicle "dual" micelle templates, as shown in Fig. 8a. TEM images indicated that the as-prepared PdAgCu hollow mesoporous nanospheres (HMSs) possess a well-defined mesoporous shell with uniform cylindrical nanochannels (Fig. 8b and c). It was proposed that the surfactant DODAC plays a very important role during the formation of PdAgCu HMSs. Surfactant-based control

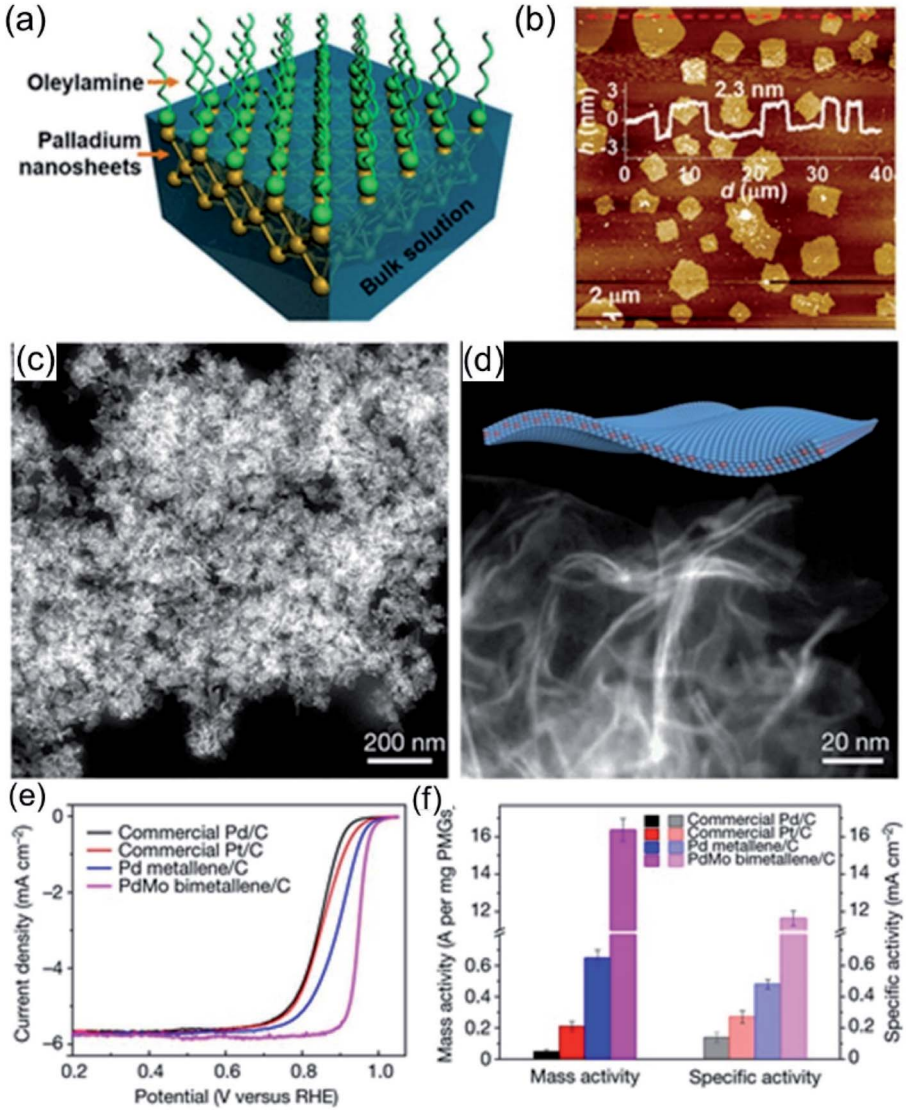

Fig. 7 (a) A schematic illustration of ILE methods for the growth of Pd nanosheets. (b) An AFM profile of the Pd nanosheets. Copyright: 2018, ACS.[95] (c and d) HADDF images of PdMo bimetallene. (e and f) The ORR testing of PdMo bimetallene in 0.1 M KOH. Copyright: 2019, Nature.[38]

experiments exhibited that other surfactants with one hydrophobic tail, such as C_{16}TAC, C_{18}TAC, C_{18}TAOC, and Pluronic F127, resulted in solid mesoporous spheres rather than hollow mesoporous nanospheres. The self-assembled "dual" DODAC micelle soft template can coordinate with metal ions to direct the formation of HMSs. Apart from the kind of surfactant used, the pH value of the reaction solution also affects the assembly behaviour of the surfactant (DODAC). Solid MS structures, HMS structures with small interiors, HMS structures, and hollow nanosphere structures with solid shells could be obtained *via* adjusting the pH value to 2.0, 3.3, 6.4, and 11.8, respectively, indicating that the DODAC micelles changed from rods to "dual" rods and vesicles, and finally to pure vesicles with an increase in the pH value. Benefiting from the highly open and channel-rich structure, the as-prepared PdAgCu HMSs possess more accessible active sites with a large ECSA (Fig. 8d), which is 3.06 times higher than that of commercial Pd black, and they have a high EOR mass activity (6.18 times higher than commercial Pd black) during the EOR in alkaline solution (Fig. 8e).

Moreover, Liu *et al.*[96] also proposed that the morphology of HMSs could be tailored into bowl-shaped mesoporous nanospheres (BMSs) with controllable spherical cone angles *via* tuning the reaction kinetics (Fig. 9a–d). Upon further adjusting the synthesis parameters (the feed amount of DODAC, temperature, pH, and metal precursor concentration), the reduction kinetics of the metal precursor on the surface of the vesicles could be controlled precisely, leading to the anisotropic island growth of PdAgCu nanocrystals on the interfaces of vesicle templates (Fig. 9e). Because of the unique structure and component advantages of BMSs, the as-prepared PdAgCu BMSs exhibited excellent electrocatalytic performance during electrocatalytic oxidation reactions (Fig. 9f and g).

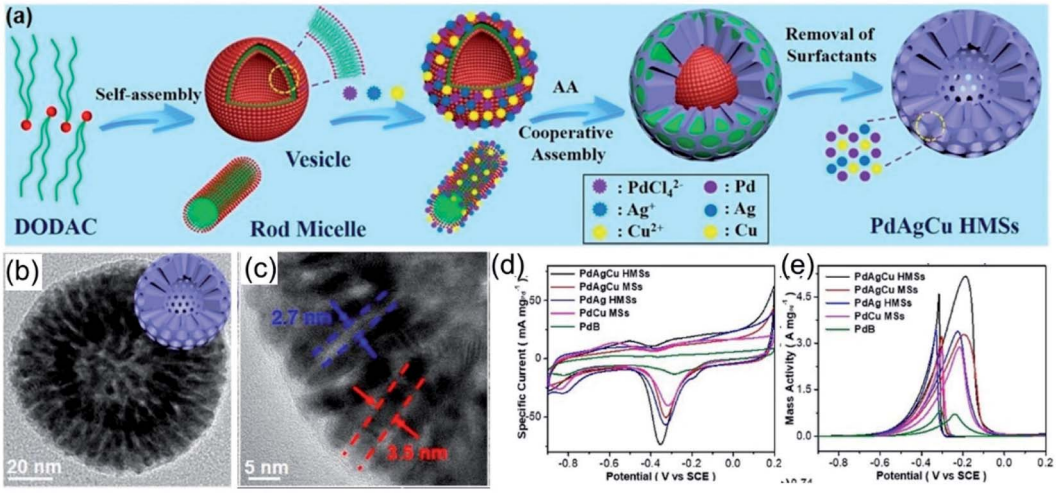

Fig. 8 (a) A schematic illustration of trimetallic PdAgCu HMSs. (b and c) High-magnification images of PdAgCu HMSs. (d) CV curves in 1.0 M KOH. (e) CV curves in 1.0 M KOH + 1.0 M CH_3CH_2OH. Copyright: 2018, ACS.[97]

Designing noble-metal nanocrystals with frame-like structures is an effective way to improve the utilization of noble-metal atoms.[24,140] Compared with other solid structures, nanocrystals with frame-like structures exhibit excellent catalytic performance owing to their high surface-atom ratios and open structures.[79,140–142] Synthesis processes for noble-metal-based nanoframes often involve a pre-synthesized template-assisted route or an in-situ-formed template-assisted route. Ni, Cu, and Co are all good template materials for noble-metal-based nanoframes.[137] Amino-based functional molecules may play an important role in dispersion and morphology control during the formation of templates. Recently, Yang, Stamenkovic *et al.*[98] reported a hollow Pt_3Ni nanoframe evolved from a $PtNi_3$ polyhedra template. Oleylamine-capped $PtNi_3$ nanocrystals make oxidized Ni more dissolvable *via* forming a soluble complex, finally leading to the formation of Pt_3Ni nanoframes (Fig. 10a and b). The optimized composition and highly open structure endow Pt_3Ni nanoframes with extraordinary ORR performance in an acid medium (the ORR catalytic activities follow the order: Pt/C < PtNi/C ≪ Pt_3Ni nanoframes). In 0.1 M $HClO_4$ electrolyte,

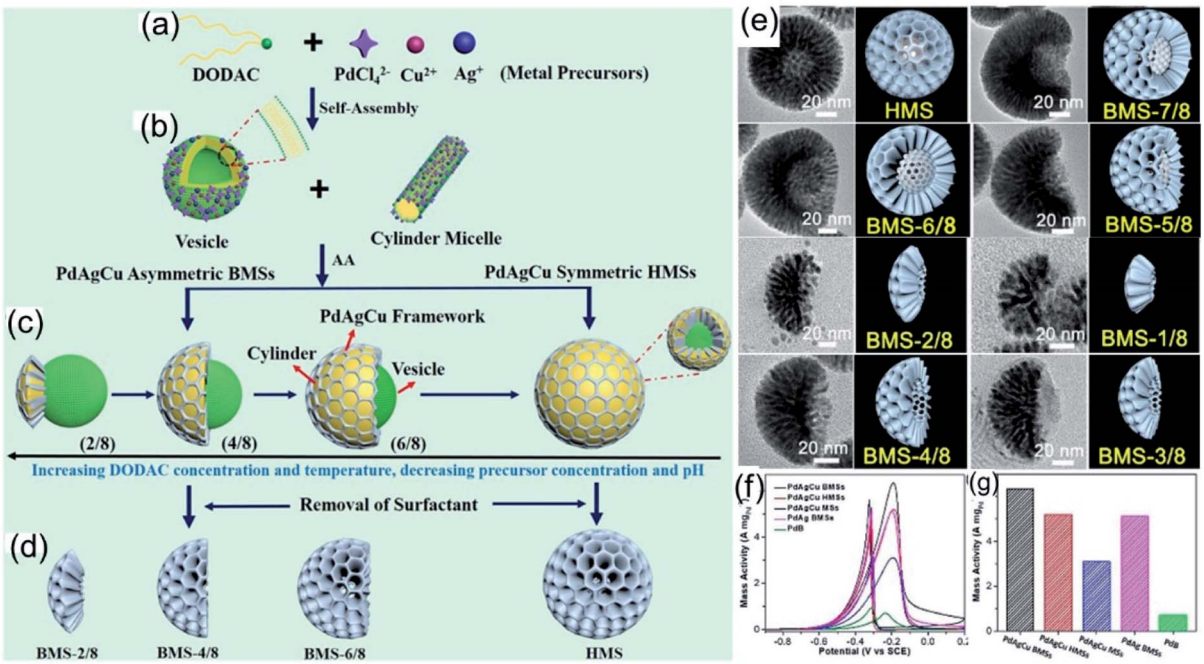

Fig. 9 (a–d) The formation of PdAgCu BMSs with controlled structural asymmetry. (e) Trimetallic PdAgCu BMSs with different DODAC concentrations. (f) CV curves and (g) calculated mass activities in 1.0 M KOH + 1.0 M CH_3CH_2OH. Copyright: 2019, ACS.[96]

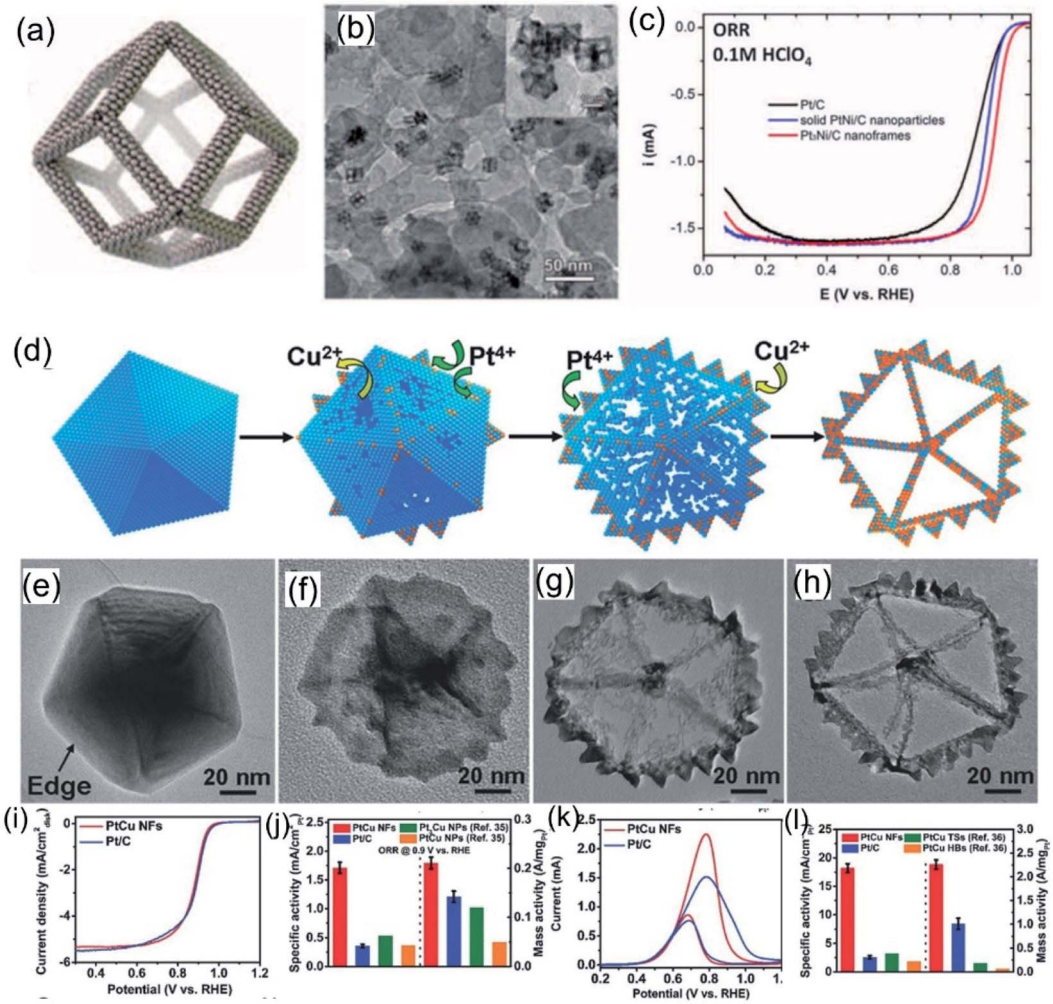

Fig. 10 (a) Annealed Pt_3Ni nanoframes. (b) Pt_3Ni nanoframes on high-surface-area carbon. (c) ORR polarization curves. Copyright: 2014, Science.[98] (d) A schematic illustration of the formation of PtCu nanoframes and (e–h) images of corresponding products after different reaction times. (i) ORR polarization curves in 0.1 M KOH. (j) Comparisons of specific activity and mass activity data. (k) CV curves in 0.5 M KOH + 1.0 M CH_3OH. (l) Comparisons of specific activity and mass activity data. Copyright: 2016, Wiley.[79]

the as-prepared Pt_3Ni nanoframes exhibit a lower Tafel slope and larger specific and mass activities compared with commercial Pt/C and PtNi/C (Fig. 10c). Huang *et al.*[143] reported a highly open rhombic dodecahedron PtCu nanoframe for the MOR. This PtCu nanoframe was produced *via* the thermal decomposition of platinum acetylacetonate and copper chloride precursors with the assistance of a 1-oleylamine/oleic acid mixture as the solvent and surfactant. Related structure-evolution investigations show that the structure of the nanoframe is closely related to the response time. Inspired by this, Wang *et al.*[107] reported Pt_3Ni tetra-hexahedron (THH) nanoframes. PtNi precursors with THH morphology were co-reduced from platinum chloride and nickel chloride precursors in 1-oleylamine and 1-octadecene at 290 °C. The high boiling points and good dispersion abilities of 1-oleylamine and 1-octadecene can effectively assist the synthesis of THHs. Similar morphologies can be seen in many reported works involving assistance from 1-oleylamine. Apart from oleylamine, Zhang *et al.*[79] reported five-fold-twinned PtCu nanoframes utilizing the assistance of glycine to form a Cu nanodecahedron template. The addition of glycine could lead to the preferential reduction of Cu, which results in the formation of the Cu nanodecahedron template. Subsequently, galvanic replacement between the Cu template and Pt^{4+} ions occurred on the surface of the Cu nanodecahedron template together with the co-reduction of Cu^{2+} and Pt^{4+} ions. Finally, five-fold-twinned PtCu nanoframes were observed. Time-dependent experiments further confirmed this formation mechanism (Fig. 10d–h). Electrochemical studies indicated that the as-prepared five-fold-twinned PtCu nanoframes exhibited higher ORR and MOR activities than commercial Pt/C and PtCu nanoparticles (Fig. 10i–l).

4. Conclusions and outlook

In summary, in recent years, research into the amino-based functional molecule assisted synthesis of noble metal nanocrystals and their applications has achieved fruitful results. In shape-control synthesis, however, the specific roles played by

amino-based functional molecules are still the subject of speculation, and related auxiliary synthesis mechanisms still need to be explored in depth. First, *in situ* characterization research relating to the morphology adjustment of noble-metal-based nanocrystals using amino-based molecules is still insufficient. A lot of in-depth research needs to be done to fully explore the mechanisms involved in the synthesis of nanocrystalline structures. Second, research into the adsorption and reaction processes relating to functional molecules on a molecular level is extremely necessary to understand the role of amino-based molecules. Exploring the adsorption of amino-based molecules on noble-metal nanocrystals at various stages, such as during nucleation and growth, would provide an understanding of mechanisms at the molecular level. It is also necessary to explore the interaction relationships between amino-based functional molecules and nanocrystals with different exposed facets. Clarifying the interaction and adsorption characteristics of amino-based functional molecules on noble-metal nanocrystals with different surface atomic arrangements could provide an effective way to better understand the mechanisms of action.

Conflicts of interest

There are no conflicts to declare.

Acknowledgements

This work was financially supported by the National Natural Science Foundation of China (21875112). The authors are also grateful for support from the National and Local Joint Engineering Research Center of Biomedical Functional Materials and a project sponsored by the Priority Academic Program Development of Jiangsu Higher Education Institutions.

Notes and references

1 Z. W. Seh, J. Kibsgaard, C. F. Dickens, I. Chorkendorff, J. K. Nørskov and T. F. Jaramillo, *Science*, 2017, **355**, eaad4998.
2 C. Kuai, Z. Xu, C. Xi, A. Hu, Z. Yang, Y. Zhang, C.-J. Sun, L. Li, D. Sokaras, C. Dong, S.-Z. Qiao, X.-W. Du and F. Lin, *Nat. Catal.*, 2020, **3**, 743–753.
3 W. Zhu, W. Chen, H. Yu, Y. Zeng, F. Ming, H. Liang and Z. Wang, *Appl. Catal., B*, 2020, **278**, 119326.
4 X. Zheng, Y. Chen, X. Zheng, G. Zhao, K. Rui, P. Li, X. Xu, Z. Cheng, S. X. Dou and W. Sun, *Adv. Energy Mater.*, 2019, **9**, 1803482.
5 L. Chen, X. Liang, X. Li, J. Pei, H. Lin, D. Jia, W. Chen, D. Wang and Y. Li, *Nano Energy*, 2020, **73**, 104784.
6 S. Fukuzumi, *Joule*, 2017, **1**, 689–738.
7 Y. M. Lee, *Nat. Energy*, 2016, **1**, 16136.
8 B. Hua, N. Yan, M. Li, Y. F. Sun, Y. Q. Zhang, J. Li, T. Etsell, P. Sarkar and J. L. Luo, *Adv. Mater.*, 2016, **28**, 8922–8926.
9 V. R. Stamenkovic, D. Strmcnik, P. P. Lopes and N. M. Markovic, *Nat. Mater.*, 2017, **16**, 57–69.
10 X. Jiang, K. Elouarzaki, Y. Tang, J. Zhou, G. Fu and J.-M. Lee, *Carbon*, 2020, **163**, 369–377.
11 H. Sun, C. Tian, G. Fan, J. Qi, Z. Liu, Z. Yan, F. Cheng, J. Chen, C. P. Li and M. Du, *Adv. Funct. Mater.*, 2020, **30**, 1910596.
12 Z.-F. Huang, J. Song, Y. Du, S. Xi, S. Dou, J. M. V. Nsanzimana, C. Wang, Z. J. Xu and X. Wang, *Nat. Energy*, 2019, **4**, 329–338.
13 H. Dotan, A. Landman, S. W. Sheehan, K. D. Malviya, G. E. Shter, D. A. Grave, Z. Arzi, N. Yehudai, M. Halabi, N. Gal, N. Hadari, C. Cohen, A. Rothschild and G. S. Grader, *Nat. Energy*, 2019, **4**, 786–795.
14 S. Z. Oener, M. J. Foster and S. W. Boettcher, *Science*, 2020, **369**, 1099–1103.
15 M. Song, Z. Zhang, Q. Li, W. Jin, Z. Wu, G. Fu and X. Liu, *J. Mater. Chem. A*, 2019, **7**, 3697–3703.
16 J. Yin, J. Jin, H. Liu, B. Huang, M. Lu, J. Li, H. Liu, H. Zhang, Y. Peng, P. Xi and C. H. Yan, *Adv. Mater.*, 2020, **32**, e2001651.
17 X. Liu, L. Zhao, H. Xu, Q. Huang, Y. Wang, C. Hou, Y. Hou, J. Wang, F. Dang and J. Zhang, *Adv. Energy Mater.*, 2020, **10**, 2001415.
18 Y. Bae, H. Song, H. Park, H. D. Lim, H. J. Kwon, Y. Ko, C. Huynh, R. Ovalle-Robles, Y. H. Kim, D. Im and K. Kang, *Adv. Energy Mater.*, 2020, **10**, 1904187.
19 C. Zhu, Z. Yin, W. Lai, Y. Sun, L. Liu, X. Zhang, Y. Chen and S.-L. Chou, *Adv. Energy Mater.*, 2018, **8**, 1802327.
20 G. Fu, Y. Tang and J.-M. Lee, *ChemElectroChem*, 2018, **5**, 1424–1434.
21 H. Xu, H. Shang, C. Wang and Y. Du, *Adv. Funct. Mater.*, 2020, **30**, 2000793.
22 Y. Li, Y. Sun, Y. Qin, W. Zhang, L. Wang, M. Luo, H. Yang and S. Guo, *Adv. Energy Mater.*, 2020, **10**, 1903120.
23 H. Li, Y. Pan, D. Zhang, Y. Han, Z. Wang, Y. Qin, S. Lin, X. Wu, H. Zhao, J. Lai, B. Huang and L. Wang, *J. Mater. Chem. A*, 2020, **8**, 2323–2330.
24 T. Kwon, M. Jun and K. Lee, *Adv. Mater.*, 2020, **32**, e2001345.
25 Y. Xia and X. Yang, *Acc. Chem. Res.*, 2017, **50**, 450–454.
26 L. Zhang, Q. Chang, H. Chen and M. Shao, *Nano Energy*, 2016, **29**, 198–219.
27 P. Strasser, *Acc. Chem. Res.*, 2016, **49**, 2658–2668.
28 C. Zhu, D. Du, A. Eychmüller and Y. Lin, *Chem. Rev.*, 2015, **115**, 8896–8943.
29 W. Yao, X. Jiang, M. Li, Y. Li, Y. Liu, X. Zhan, G. Fu and Y. Tang, *Appl. Catal., B*, 2021, **282**, 119595.
30 Z. Teng, M. Li, Z. Li, Z. Liu, G. Fu and Y. Tang, *Mater. Today Energy*, 2021, **19**, 100596.
31 G. Fu, X. Jiang, L. Tao, Y. Chen, J. Lin, Y. Zhou, Y. Tang and T. Lu, *Langmuir*, 2013, **29**, 4413–4420.
32 G. Fu, K. Wu, X. Jiang, L. Tao, Y. Chen, J. Lin, Y. Zhou, S. Wei, Y. Tang, T. Lu and X. Xia, *Phys. Chem. Chem. Phys.*, 2013, **15**, 3793–3802.
33 Z. Li, X. Jiang, X. Wang, J. Hu, Y. Liu, G. Fu and Y. Tang, *Appl. Catal., B*, 2020, **277**, 119135.
34 Q. Shao, F. Li, Y. Chen and X. Huang, *Adv. Mater. Interfaces*, 2018, **5**, 1800486.

35 B. Lim, M. Jiang, J. Tao, P. H. C. Camargo, Y. Zhu and Y. Xia, *Adv. Funct. Mater.*, 2009, **19**, 189–200.
36 V. Mazumder, Y. Lee and S. Sun, *Adv. Funct. Mater.*, 2010, **20**, 1224–1231.
37 M. Escudero-Escribano, A. Verdaguer-Casadevall, P. Malacrida, U. Gronbjerg, B. P. Knudsen, A. K. Jepsen, J. Rossmeisl, I. E. Stephens and I. Chorkendorff, *J. Am. Chem. Soc.*, 2012, **134**, 16476–16479.
38 M. Luo, Z. Zhao, Y. Zhang, Y. Sun, Y. Xing, F. Lv, Y. Yang, X. Zhang, S. Hwang, Y. Qin, J. Y. Ma, F. Lin, D. Su, G. Lu and S. Guo, *Nature*, 2019, **574**, 81–85.
39 C. Zhu, D. Wen, M. Oschatz, M. Holzschuh, W. Liu, A. K. Herrmann, F. Simon, S. Kaskel and A. Eychmuller, *Small*, 2015, **11**, 1430–1434.
40 H. Zhu, Y. Cai, F. Wang, P. Gao and J. Cao, *ACS Appl. Mater. Interfaces*, 2018, **10**, 22156–22166.
41 T. H. Yang, Y. Shi, A. Janssen and Y. Xia, *Angew. Chem., Int. Ed.*, 2019, **59**, 15378–15401.
42 J. Zhou, J. Li, L. Zhang, S. Song, Y. Wang, X. Lin, S. Gu, X. Wu, T.-C. Weng, J. Wang and S. Zhang, *J. Phys. Chem. C*, 2018, **122**, 14447–14458.
43 W. Gao, Y. Hou, Z. D. Hood, X. Wang, K. More, R. Wu, Y. Xia, X. Pan and M. Chi, *Nano Lett.*, 2018, **18**, 7004–7013.
44 M. Meng, Z. Fang, C. Zhang, H. Su, R. He, R. Zhang, H. Li, Z. Y. Li, X. Wu, C. Ma and J. Zeng, *Nano Lett.*, 2016, **16**, 3036–3041.
45 N. F. Yu, N. Tian, Z. Y. Zhou, L. Huang, J. Xiao, Y. H. Wen and S. G. Sun, *Angew. Chem., Int. Ed.*, 2014, **53**, 5097–5101.
46 Y. Qi, T. Bian, S. I. Choi, Y. Jiang, C. Jin, M. Fu, H. Zhang and D. Yang, *Chem. Commun.*, 2014, **50**, 560–562.
47 C. Luan, Q. X. Zhou, Y. Wang, Y. Xiao, X. Dai, X. L. Huang and X. Zhang, *Small*, 2017, **13**, 1702617.
48 X. Yan, X. Hu, G. Fu, L. Xu, J. M. Lee and Y. Tang, *Small*, 2018, **14**, e1703940.
49 Y. Yang, M. Luo, W. Zhang, Y. Sun, X. Chen and S. Guo, *Chem*, 2018, **4**, 2054–2083.
50 G. Fu, X. Yan, Z. Cui, D. Sun, L. Xu, Y. Tang, J. B. Goodenough and J.-M. Lee, *Chem. Sci.*, 2016, **7**, 5414–5420.
51 A. R. Poerwoprajitno, L. Gloag, S. Cheong, J. J. Gooding and R. D. Tilley, *Nanoscale*, 2019, **11**, 18995–19011.
52 H. Xu, H. Shang, C. Wang and Y. Du, *Adv. Funct. Mater.*, 2020, **30**, 2006317.
53 S. J. Guo and E. K. Wang, *Nano Today*, 2011, **6**, 240–264.
54 B. Lim and Y. Xia, *Angew. Chem., Int. Ed.*, 2011, **50**, 76–85.
55 J. Park, S. Choi, A. Oh, H. Jin, J. Joo, H. Baik and K. Lee, *Nanoscale Horiz.*, 2019, **4**, 727–734.
56 L. Sun, D. Zhang, Y. Sun, S. Wang and J. Cai, *Adv. Funct. Mater.*, 2018, **28**, 1707231.
57 X. Zhao, L. Dai, Q. Qin, F. Pei, C. Hu and N. Zheng, *Small*, 2017, **13**, 1602970.
58 Z. Luo, J. Ahn and D. Qin, *Nanoscale*, 2019, **11**, 6710–6718.
59 G.-T. Fu, B.-Y. Xia, R.-G. Ma, Y. Chen, Y.-W. Tang and J.-M. Lee, *Nano Energy*, 2015, **12**, 824–832.
60 G. Fu, Z. Liu, Y. Chen, J. Lin, Y. Tang and T. Lu, *Nano Res.*, 2014, **7**, 1205–1214.
61 Y. Yan, X. Li, M. Tang, H. Zhong, J. Huang, T. Bian, Y. Jiang, Y. Han, H. Zhang and D. Yang, *Adv. Sci.*, 2018, **5**, 1800430.
62 M. B. Lim, J. L. Hanson, L. Vandsburger, P. B. Roder, X. Zhou, B. E. Smith, F. S. Ohuchi and P. J. Pauzauskie, *J. Mater. Chem. A*, 2018, **6**, 5644–5651.
63 L. Figueroa-Cosme, Z. D. Hood, K. D. Gilroy and Y. Xia, *J. Mater. Chem. C*, 2018, **6**, 4677–4682.
64 S. Kondo, M. Nakamura, N. Maki and N. Hoshi, *J. Phys. Chem. C*, 2009, **113**, 12625–12628.
65 N. Guo, H. Xue, A. Bao, Z. Wang, J. Sun, T. Song, X. Ge, W. Zhang, K. Huang, F. He and Q. Wang, *Angew. Chem., Int. Ed.*, 2020, **59**, 13778–13784.
66 Y. Chen, Y. Yang, G. Fu, L. Xu, D. Sun, J.-M. Lee and Y. Tang, *J. Mater. Chem. A*, 2018, **6**, 10632–10638.
67 X. Xu, X. Zhang, H. Sun, Y. Yang, X. Dai, J. Gao, X. Li, P. Zhang, H. H. Wang, N. F. Yu and S. G. Sun, *Angew. Chem., Int. Ed.*, 2014, **53**, 12522–12527.
68 Y. Wang, X. Jiang, G. Fu, Y. Li, Y. Tang, J.-M. Lee and Y. Tang, *ACS Appl. Mater. Interfaces*, 2019, **11**, 34869–34877.
69 C. Fan, Z. Huang, C. Wang, X. Hu, X. Qiu, P. She, D. Sun and Y. Tang, *Chemistry*, 2019, **25**, 4920–4926.
70 G. Fu, K. Wu, J. Lin, Y. Tang, Y. Chen, Y. Zhou and T. Lu, *J. Phys. Chem. C*, 2013, **117**, 9826–9834.
71 G. Fu, W. Han, L. Yao, J. Lin, S. Wei, Y. Chen, Y. Tang, Y. Zhou, T. Lu and X. Xia, *J. Phys. Chem.*, 2012, **22**, 17604–17611.
72 G. Fu, X. Jiang, L. Ding, L. Tao, Y. Chen, Y. Tang, Y. Zhou, S. Wei, J. Lin and T. Lu, *Appl. Catal., B*, 2013, **138–139**, 167–174.
73 Z. Li, Y. Chen, G. Fu, Y. Chen, D. Sun, J. M. Lee and Y. Tang, *Nanoscale*, 2019, **11**, 2974–2980.
74 G. Fu, M. Gong, Y. Tang, L. Xu, D. Sun and J.-M. Lee, *J. Mater. Chem. A*, 2015, **3**, 21995–21999.
75 Y. Chen, X. Jiang, Y. Li, P. Li, Q. Liu, G. Fu, L. Xu, D. Sun and Y. Tang, *Adv. Mater. Interfaces*, 2018, **5**, 1701015.
76 Z. Han, A. J. Wang, L. Zhang, Z. G. Wang, K. M. Fang, Z. Z. Yin and J. J. Feng, *J. Colloid Interface Sci.*, 2019, **554**, 512–519.
77 X.-Y. Huang, A.-J. Wang, X.-F. Zhang, L. Zhang and J.-J. Feng, *ACS Appl. Energy Mater.*, 2018, **2018**(1), 5779–5786.
78 Z. Zhang, Y. Yang, F. Nosheen, P. Wang, J. Zhang, J. Zhuang and X. Wang, *Small*, 2013, **9**, 3063–3069.
79 Z. Zhang, Z. Luo, B. Chen, C. Wei, J. Zhao, J. Chen, X. Zhang, Z. Lai, Z. Fan, C. Tan, M. Zhao, Q. Lu, B. Li, Y. Zong, C. Yan, G. Wang, Z. J. Xu and H. Zhang, *Adv. Mater.*, 2016, **28**, 8712–8717.
80 H. Zhang, X. Qiu, Y. Chen, S. Wang, S. E. Skrabalak and Y. Tang, *Small*, 2020, **16**, e1906026.
81 P. Zhang, X. Dai, X. Zhang, Z. Chen, Y. Yang, H. Sun, X. Wang, H. Wang, M. Wang, H. Su, D. Li, X. Li and Y. Qin, *Chem. Mater.*, 2015, **27**, 6402–6410.
82 J. Lai and S. Guo, *Small*, 2017, **13**, 1702156.
83 L. Zhang, J. Zhang, Q. Kuang, S. Xie, Z. Jiang, Z. Xie and L. Zheng, *J. Am. Chem. Soc.*, 2011, **133**, 17114–17117.
84 X.-F. Zhang, H.-B. Meng, H.-Y. Chen, J.-J. Feng, K.-M. Fang and A.-J. Wang, *J. Alloys Compd.*, 2019, **786**, 232–239.

85 Y. Chen, G. Fu, Y. Li, Q. Gu, L. Xu, D. Sun and Y. Tang, *J. Mater. Chem. A*, 2017, **5**, 3774–3779.
86 G. Fu, H. Liu, N. You, J. Wu, D. Sun, L. Xu, Y. Tang and Y. Chen, *Nano Res.*, 2016, **9**, 755–765.
87 X. F. Zhang, Y. Chen, L. Zhang, A. J. Wang, L. J. Wu, Z. G. Wang and J. J. Feng, *J. Colloid Interface Sci.*, 2018, **516**, 325–331.
88 H. Li, X. Wu, X. Tao, Y. Lu and Y. Wang, *Small*, 2020, **16**, e2001135.
89 M. Gong, Z. Deng, D. Xiao, L. Han, T. Zhao, Y. Lu, T. Shen, X. Liu, R. Lin, T. Huang, G. Zhou, H. Xin and D. Wang, *ACS Catal.*, 2019, **9**, 4488–4494.
90 N. Zhang, Y. Feng, X. Zhu, S. Guo, J. Guo and X. Huang, *Adv. Mater.*, 2017, **29**, 1603774.
91 K. Jiang, Q. Shao, D. Zhao, L. Bu, J. Guo and X. Huang, *Adv. Funct. Mater.*, 2017, **27**, 1700830.
92 W. Wang, X. Chen, X. Zhang, J. Ye, F. Xue, C. Zhen, X. Liao, H. Li, P. Li, M. Liu, Q. Kuang, Z. Xie and S. Xie, *Nano Energy*, 2020, **71**, 104623.
93 K. Guo, Y. Liu, M. Han, D. Xu and J. Bao, *Chem. Commun.*, 2019, **55**, 11131–11134.
94 F. Saleem, Z. Zhang, X. Cui, Y. Gong, B. Chen, Z. Lai, Q. Yun, L. Gu and H. Zhang, *J. Am. Chem. Soc.*, 2019, **141**, 14496–14500.
95 X. Yin, Q. Chen, P. Tian, P. Zhang, Z. Zhang, P. M. Voyles and X. Wang, *Chem. Mater.*, 2018, **30**, 3308–3314.
96 H. Lv, D. Xu, L. Sun, J. Henzie, A. Lopes, Q. Gu, Y. Yamauchi and B. Liu, *Nano Lett.*, 2019, **19**, 3379–3385.
97 H. Lv, A. Lopes, D. Xu and B. Liu, *ACS Cent. Sci.*, 2018, **4**, 1412–1419.
98 C. Chen, Y. Kang, Z. Huo, Z. Zhu, W. Huang, H. L. Xin, J. D. Snyder, D. Li, J. A. Herron, M. Mavrikakis, M. Chi, K. L. More, Y. Li, N. M. Markovic, G. A. Somorjai, P. Yang and V. R. Stamenkovic, *Science*, 2014, **343**, 1339–1343.
99 S. I. Choi, S. Xie, M. Shao, N. Lu, S. Guerrero, J. H. Odell, J. Park, J. Wang, M. J. Kim and Y. Xia, *ChemSusChem*, 2014, **7**, 1476–1483.
100 M. Nesselberger, S. Ashton, J. C. Meier, I. Katsounaros, K. J. Mayrhofer and M. Arenz, *J. Am. Chem. Soc.*, 2011, **133**, 17428–17433.
101 Q. Yuan, H. A. Doan, L. C. Grabow and S. R. Brankovic, *J. Am. Chem. Soc.*, 2017, **139**, 13676–13679.
102 S. M. Rogers, C. R. A. Catlow, C. E. Chan-Thaw, A. Chutia, N. Jian, R. E. Palmer, M. Perdjon, A. Thetford, N. Dimitratos, A. Villa and P. P. Wells, *ACS Catal.*, 2017, **7**, 2266–2274.
103 H. Huang, Y. Wang, A. Ruditskiy, H.-C. Peng, X. Zhao, L. Zhang, J. Liu, Z. Ye and Y. Xia, *ACS Nano*, 2014, **8**, 7041–7050.
104 Y. Zhang, X. Zhu, J. Guo and X. Huang, *ACS Appl. Mater. Interfaces*, 2016, **8**, 20642–20649.
105 Z. Quan, Y. Wang and J. Fang, *Acc. Chem. Res.*, 2012, **46**, 191–202.
106 Y. Wang, M. Zheng, H. Sun, X. Zhang, C. Luan, Y. Li, L. Zhao, H. Zhao, X. Dai, J.-Y. Ye, H. Wang and S.-G. Sun, *Appl. Catal., B*, 2019, **253**, 11–20.
107 C. Wang, L. Zhang, H. Yang, J. Pan, J. Liu, C. Dotse, Y. Luan, R. Gao, C. Lin, J. Zhang, J. P. Kilcrease, X. Wen, S. Zou and J. Fang, *Nano Lett.*, 2017, **17**, 2204–2210.
108 H. Xu, H. Shang, C. Wang and Y. Du, *Adv. Funct. Mater.*, 2020, **30**, 2006317.
109 H. Xu, H. Shang, C. Wang and Y. Du, *Adv. Funct. Mater.*, 2020, **30**, 2000793.
110 G.-T. Fu, R. Wu, C. Liu, J. Lin, D.-M. Sun and Y.-W. Tang, *RSC Adv.*, 2015, **5**, 18111–18115.
111 X. Sun, B. Huang, X. Cui, B. E, Y. Feng and X. Huang, *ChemCatChem*, 2018, **10**, 931–935.
112 Y. Zhu, L. Bu, Q. Shao and X. Huang, *ACS Catal.*, 2020, **10**, 3455–3461.
113 S. Bai, L. Bu, Q. Shao, X. Zhu and X. Huang, *J. Am. Chem. Soc.*, 2018, **140**, 8384–8387.
114 P. Wang, X. Zhang, J. Zhang, S. Wan, S. Guo, G. Lu, J. Yao and X. Huang, *Nat. Commun.*, 2017, **8**, 14580.
115 K. Jiang, D. Zhao, S. Guo, X. Zhang, X. Zhu, J. Guo, G. Lu and X. Huang, *Sci. Adv.*, 2017, **3**, e1601705.
116 Y. Zhu, X. Zhu, L. Bu, Q. Shao, Y. Li, Z. Hu, C. T. Chen, C. W. Pao, S. Yang and X. Huang, *Adv. Funct. Mater.*, 2020, **30**, 2004310.
117 P. Wang, Q. Shao, J. Guo, L. Bu and X. Huang, *Chem. Mater.*, 2020, **32**, 3144–3149.
118 Y. Zhu, L. Bu, Q. Shao and X. Huang, *ACS Catal.*, 2019, **9**, 6607–6612.
119 Y. Pi, J. Guo, Q. Shao and X. Huang, *Chem. Mater.*, 2018, **30**, 8571–8578.
120 N. Zhang, Y. Zhu, Q. Shao, X. Zhu and X. Huang, *J. Mater. Chem. A*, 2017, **5**, 18977–18983.
121 W. Lu, X. Xia, X. Wei, M. Li, M. Zeng, J. Guo and S. Cheng, *ACS Appl. Mater. Interfaces*, 2020, **12**, 21569–21578.
122 H. Lv, Y. Wang, A. Lopes, D. Xu and B. Liu, *Appl. Catal., B*, 2019, **249**, 116–125.
123 H. Lv, L. Sun, L. Zou, D. Xu, H. Yao and B. Liu, *Chem. Sci.*, 2019, **10**, 1986–1993.
124 H. Lv, L. Sun, D. Xu, J. Henzie, Y. Yamauchi and B. Liu, *J. Mater. Chem. A*, 2019, **7**, 24877–24883.
125 H. Lv, L. Sun, A. Lopes, D. Xu and B. Liu, *J. Phys. Chem. Lett.*, 2019, **10**, 5490–5498.
126 L. Bu, S. Guo, X. Zhang, X. Shen, D. Su, G. Lu, X. Zhu, J. Yao, J. Guo and X. Huang, *Nat. Commun.*, 2016, **7**, 11850.
127 L. Ruan, E. Zhu, Y. Chen, Z. Lin, X. Huang, X. Duan and Y. Huang, *Angew. Chem., Int. Ed.*, 2013, **52**, 12577–12581.
128 Y. Li and S. Guo, *Nano Today*, 2019, **28**, 100774.
129 Q. Sun, H. Xu and Y. Du, *ChemSusChem*, 2020, **13**, 2540–2551.
130 G. H. Jeong, S. P. Sasikala, T. Yun, G. Y. Lee, W. J. Lee and S. O. Kim, *Adv. Mater.*, 2020, **32**, e1907006.
131 J. Fan, J. Wu, X. Cui, L. Gu, Q. Zhang, F. Meng, B. H. Lei, D. J. Singh and W. Zheng, *J. Am. Chem. Soc.*, 2020, **142**, 3645–3651.
132 G. Fu, X. Jiang, M. Gong, Y. Chen, Y. Tang, J. Lin and T. Lu, *Nanoscale*, 2014, **6**, 8226–8234.
133 G. Fu, H. Liu, N. You, J. Wu, D. Sun, L. Xu, Y. Tang and Y. Chen, *Nano Res.*, 2016, **9**, 755–765.

134 S. Yang, G. Chen, A. G. Ricciardulli, P. Zhang, Z. Zhang, H. Shi, J. Ma, J. Zhang, P. W. M. Blom and X. Feng, *Angew. Chem., Int. Ed.*, 2020, **59**, 465–470.
135 S. Yin, H. Wang, K. Deng, Z. Dai, Z. Wang, Y. Xu, X. Li, H. Xue and L. Wang, *Chemistry*, 2019, **25**, 5316–5321.
136 J. Lee and J. Y. Chang, *RSC Adv.*, 2018, **8**, 25277–25282.
137 L.-M. Lyu, Y.-C. Kao, D. A. Cullen, B. T. Sneed, Y.-C. Chuang and C.-H. Kuo, *Chem. Mater.*, 2017, **29**, 5681–5692.
138 Y. Zhao, J. Zhang, W. Li, C. Zhang and B. Han, *Chem. Commun.*, 2009, **17**, 2365–2367.
139 X. W. Lou, L. A. Archer and Z. Yang, *Adv. Mater.*, 2008, **20**, 3987–4019.
140 X. Wang, A. Ruditskiy and Y. Xia, *Natl. Sci. Rev.*, 2016, **3**, 520–533.
141 G. Gruzel, S. Arabasz, M. Pawlyta and M. Parlinska-Wojtan, *Nanoscale*, 2019, **11**, 5355–5364.
142 W. Ye, S. Kou, X. Guo, F. Xie, H. Sun, H. Lu and J. Yang, *Nanoscale*, 2015, **7**, 9558–9562.
143 J. Ding, X. Zhu, L. Bu, J. Yao, J. Guo, S. Guo and X. Huang, *Chem. Commun.*, 2015, **51**, 9722–9725.